Science of the Total Environment 939 (2024) 173599

Contents lists available at ScienceDirect

Science of the Total Environment

journal homepage: www.elsevier.com/locate/scitotenv

North-south discrepancy in the contributors to CB153 accumulation in the deep water of the Sea of Japan

Min Yang [a], Xinyu Guo [b,c,*], Junyong Zheng [d], Yasumasa Miyazawa [c]

[a] State Key Laboratory of Satellite Ocean Environment Dynamics, Second Institute of Oceanography, Ministry of Natural Resources, 36 Baochu Road, Hangzhou 310012, China
[b] Center for Marine Environmental Studies, Ehime University, 2-5 Bunkyo-Cho, Matsuyama 790-8577, Japan
[c] Application Laboratory, Japan Agency for Marine-Earth Science and Technology, 3173-25, Showa-machi, Kanazawa-ku, Yokohama-City, Kanagawa 236-0001, Japan
[d] College of Oceanic and Atmospheric Sciences, Ocean University of China, 238 Songling Road, Qingdao 266100, China

HIGHLIGHTS

- CB153 concentration is the highest in the 100–600 m layer in the Sea of Japan.
- A fully coupled 3D hydrodynamic-ecological-PCBs model was developed.
- Biological pump accelerates the accumulation of CB153 in the northern Sea of Japan.
- Vertical advection enhances the accumulation of CB153 in the southern Sea of Japan.

GRAPHICAL ABSTRACT

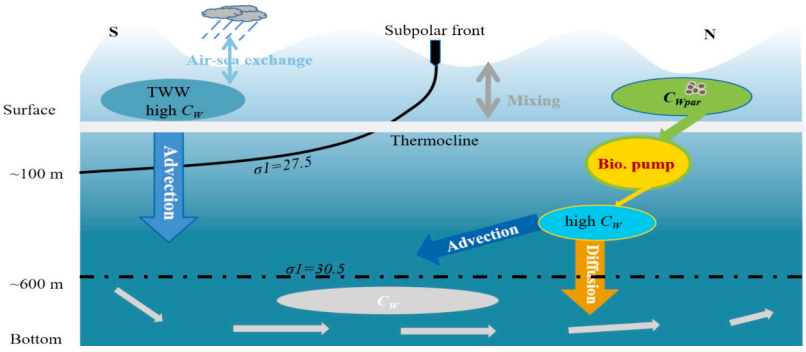

ARTICLE INFO

Editor: Paromita Chakraborty

Keywords:
Ocean model
Oceanic biological pump
Vertical advection
Intermediate water
Thermocline

ABSTRACT

The deep-water environment and its ecosystem are becoming the ultimate sinks for Polychlorinated Biphenyls (PCBs). A three-dimensional hydrodynamic-ecosystem-PCB coupled model was applied to the Sea of Japan (SoJ), where deep water is isolated from the surrounding oceans, to elucidate the accumulation processes of CB153 and assess the contributions of physical and biological processes to the accumulation. We suggest that the dissolved CB153 concentration formed a three-layer vertical structure in the SoJ: the highest concentration is in the intermediate layer (100–600 m), followed by those in the deep (600 m to the bottom) and surface layers (0–100 m). Different accumulation mechanisms in the northern and southern SoJ were discovered. The oceanic biological pump enhances the accumulation in the northern SoJ by taking CB153 out of the thermocline in summer and contributes 70 % to the accumulation in the intermediate layer; while the vertical advection contributes 70 % to the accumulation in the intermediate and deep layer in the southern SoJ.

* Corresponding author at: Center for Marine Environmental Studies, Ehime University, 2-5 Bunkyo-Cho, Matsuyama 790-8577, Japan.
E-mail address: guo.xinyu.mz@ehime-u.ac.jp (X. Guo).

https://doi.org/10.1016/j.scitotenv.2024.173599
Received 8 January 2024; Received in revised form 25 May 2024; Accepted 26 May 2024
Available online 29 May 2024

1. Introduction

Polychlorinated biphenyls (PCBs) are highly toxic and readily accumulated by marine mammals owing to their lipophilicity, which detrimentally impacts the immune system, thus posing a critical risk to the marine ecosystem (Friedman and Selin, 2016; Jepson et al., 2016). High PCBs concentrations have been detected in deep-sea organisms (de Brito et al., 2002; Storelli et al., 2009), for example in fish at a depth of 10,000 m in the Mariana Trench, Antarctic, and Arctic waters (Corsolini et al., 2017; Jamieson et al., 2017). Observations also indicate that PCBs are much more concentrated in deep-sea fish than in surface fish. In the Atlantic Ocean, PCBs concentrations at a depth of 800 m are 10 times higher than those in surface fish, and this factor is approximately 4 for the Pacific Ocean (Froescheis et al., 2000).

The Sea of Japan (SoJ) is a semi-closed marginal sea in the northwestern Pacific Ocean, surrounded by the Japanese Archipelago and Far Eastern Eurasia, and characterized by its marked bathymetric isolated geography (Gamo et al., 2014). The average depth of the sea is approximately 1667 m, and the maximum depth is approximately 3800 m (Fig. 1). It is connected to the northwestern Pacific Ocean through the Tsushima, Tsugaru, Soya, and Tartar Straits (Lee et al., 2008; Oba and Irino, 2012), and the maximum depth of these four straits is <150 m. Such bowl-shaped bathymetry separates its intermediate and deep water masses from the adjacent seas and confines the effect of flows through the straits to the upper 200 m (Isobe, 2020; Oba and Irino, 2012; Yanagi, 2002). The upper circulation of the SoJ consists of the Tsushima Warm Current and the Liman Cold Current. Water below the thermocline is Japan Sea Proper Water, which has a very narrow temperature and salinity range (Gamo et al., 2014).

The SoJ is a possible candidate for PCB sinks due to the heavy human activities around the sea. The high primary productivity in the subpolar front region of the SoJ may enhance the vertical sinking of particle-associated pollutants such as PCBs (Takahashi et al., 2014). In addition, the semi-enclosed topography of the sea isolates deep water from the surrounding oceans, which is conducive to PCB accumulation in deep water. The concentration of PCBs in fish in the SoJ was reported to be 2–9 times higher than that in the North Pacific Ocean (Ueno et al., 2003). In addition, crab (king crab, snow crab, etc.) is one of the deepwater species in the SoJ (Kanawa et al., 2014; Yosho et al., 2009), and contributes significantly to the income from fisheries (Dvoretsky and Dvoretsky, 2018). However, high PCBs concentrations can lower the resilience of crabs in deep water, which may be one reason why crab catches have declined in recent years.

Few studies have been conducted on the concentration of PCBs in the deep ocean, and available measurements are mainly located in the Atlantic Ocean and its marginal seas, the Arctic Ocean, and the Southern Ocean (Lohmann et al., 2006; Maldonado and Bayona, 2002; Schulz-Bull et al., 1998; Sobek and Gustafsson, 2014; Sun et al., 2016). The only study that reported the presence of PCBs in the SoJ showed that the vertical distribution of dissolved PCBs concentration was high in middle-depth water and low in both surface and bottom waters (Kannan et al., 1998). However, the mechanisms underlying the formation of these structures remain unclear. High organophosphate esters (OPEs) concentration was observed below the surface water in the Changjiang River estuary where the fronts/upwelling activity could induce phytoplankton blooms, indicating the combined impacts of hydrological and biogeochemical processes (Zhang et al., 2023).

Clarifying the accumulation of PCBs and their mechanisms is important for the conservation of deep-sea ecosystems and fishery resources in marginal seas. However, most ocean models of PCBs have focused on the biochemical processes in surface water (Dachs et al., 2002; Jurado et al., 2004, 2005). The extent and mechanism of PCBs accumulation in deep water are still poorly investigated. In this study, we established a three-dimensional high-resolution hydrodynamic-ecosystem-PCBs coupled model and targeted at the SoJ to examine the accumulation of PCBs in the deep sea. The relative contributions of physical and biological processes to the vertical transport of PCBs are therefore quantitatively discussed.

2. Materials and methods

We use the three-dimensional hydrodynamic-ecosystem-PCBs coupled model to depict the accumulation of CB153 in deep water, which has been successfully applied to the northwestern Pacific Ocean (Yang et al., 2022). The hydrodynamic module provides daily water temperature, current velocity in three directions, and the horizontal and vertical eddy diffusivity coefficients. This module has been demonstrated to effectively reproduce the oceanic conditions of the Sea of Japan (Miyazawa et al., 2017). The ecosystem module provides the daily biomass and the related biological parameters such as the mortality rate

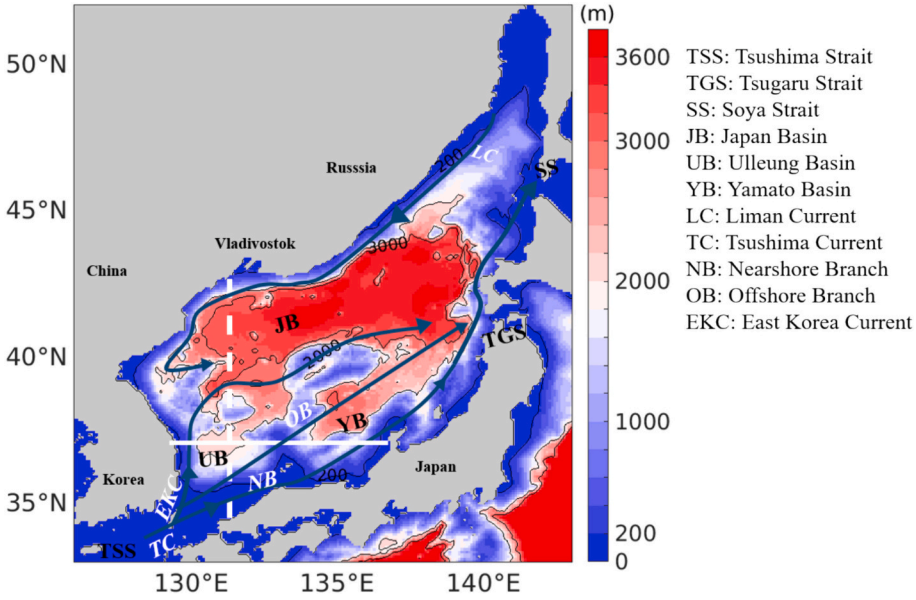

Fig. 1. Model domain and bathymetry of the Sea of Japan (SoJ). White dashed (solid) line denotes the 131°E (37°N) section, and the grey solid lines denotes the ocean currents in the SoJ.

of phytoplankton, and the decomposition rate and sinking velocity of the detritus. We included dissolved and particulate-bound PCBs in the PCB module, and the concentration of particulate-bound PCBs depends on the concentrations of phytoplankton and detritus. Mass exchange and chemical degradation are the principal processes considered in the PCBs module. Mass exchange processes include advection and diffusion, biogeochemical processes, and air-sea exchange. The hydrodynamic, ecosystem, and PCBs modules and atmospheric boundary conditions for the PCBs module in the northwestern Pacific Ocean are provided in Supporting Information (Text S1–S4). In this study, two main improvements to the model were made: (a) the processes for the self-degradation of dissolved PCBs were modified by including the degradation of dissolved CB153 due to photolysis, which essentially introduced the dependence of photolytic degradation of PCBs on water depth; and (b) the biological processes of PCBs included not only the uptake and adsorption of CB153 by phytoplankton but also by detritus.

PCBs degrade through both photolytic and biological processes (Abramowicz, 1990; Sinkkonen and Paasivirta, 2000). Previous research suggests microbial degradation of PCBs is approximately one order of magnitude lower than photolytic degradation (Sinkkonen and Paasivirta, 2000; Zhang et al., 2015). We thus considered only the photolytic process (Eq. (1)):

$$K_{deg} = k_{base,T}\frac{RAD_z}{RAD_{surf}} \quad (1)$$

where $k_{base,T}$ is the temperature-adjusted degradation base rate (s^{-1}), RAD_{surf} and RAD_z are the shortwave radiation intensity (W m^{-2}) at the surface and at depth z, respectively (Wagner et al., 2019).

The contribution of each PCB congener to deep-sea fish is different. Highly chlorinated congeners such as hexa-CBs (CB138 and CB153) are the most abundant, followed by hepta-CBs (CB180) and less chlorinated congeners (CB28 and CB52) (Froescheis et al., 2000; Storelli et al., 2009). Therefore, CB153 was selected as the target compound in this study. The initial values for the dissolved, phytoplankton, and detritus phases of CB153 concentrations in the ocean were set to zero. Under the climatological data of the physical, ecosystem module, and the climatological concentration of atmospheric CB153, the PCB module was solved offline using these modules and integrated over 21 years. During the 21 years of calculation, the model results in the upper 200 m layer were almost the same in the 20th and 21st years, indicating that the model essentially reached a steady state in the upper layer. Hereafter, this calculation is referred to as the control run, and the results for the last year were analyzed.

This model was previously validated by comparing its results with the observations of PCBs concentrations in various oceans and their marginal seas (Yang et al., 2022). And both the dissolved and particulate concentrations of PCBs on the northwestern Pacific Ocean surface given by the ocean module are within the range of known observations. Although our model covers the northwestern Pacific Ocean, we focused on the SoJ (33–52°N, 126–143°E; Fig. 1) in this study. Sensitivity simulations were conducted to examine the roles of physical (advection and diffusion) and biological processes in the accumulation of PCBs in the SoJ.

3. Results and discussions

3.1. Temporal-spatial distribution of CB153 concentration in the SoJ

The annual mean distributions of the dissolved and particulate CB153 concentrations are different (Fig. 2). The concentration of dissolved CB153 in the sea surface decreases from the southern area (~0.5 pg L^{-1}) to the northern area (~0.3 pg L^{-1}) (Fig. 2a). The CB153 concentration in the 50 m layer is lower than 0.3 pg L^{-1} in the western Japan Basin (Fig. 2b). However, there is a significantly high concentration (~0.7 pg L^{-1}) distributed in the middle layer from 100 to 600 m

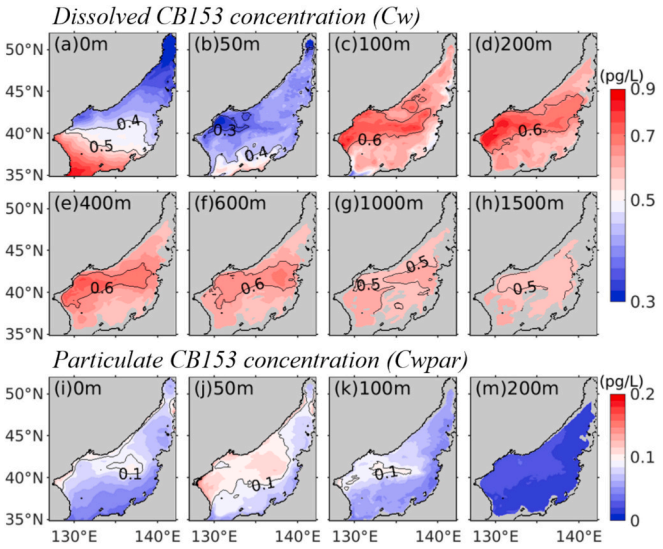

Fig. 2. Horizontal distributions of annual mean concentrations of dissolved CB153 (a–h) and particulate CB153 (i–m) at different depths in the SoJ.

depth in the Japan Basin (Fig. 2c–f), which is approximately twice that in the upper 100 m layer. The CB153 concentration in the deep layer (600–1500 m, ~0.5 pg L^{-1}) is lower than that in the middle layer (100–600 m) but is higher than that in the upper 100 m layer, and this pattern is uniformly distributed across the SoJ (Fig. 2g, h). The distribution and magnitude of the dissolved concentration in the layers deeper than 1500 m are similar to those in the 1500 m layer; thus, these results are not shown in Fig. 2. The concentration of dissolved CB153 showed a three-layer structure from the sea surface to the deep layer, which allows us to divide the SoJ into three layers: the surface layer (0–100 m), intermediate layer (100–600 m), and deep layer (600 m to the bottom).

The annual mean concentration of particulate CB153 is lower than that of dissolved CB153 and is mainly distributed in the upper 200 m (Fig. 2i–m). The 50–100 m layer shows the highest concentration of ~0.1 pg L^{-1} in the Japan Basin, while the sea surface shows a lower concentration. Particulate CB153 includes phytoplankton and detritus bound CB153, and the concentration of phytoplankton bound is approximately twice that of the detritus bound.

Due to the lack of vertical observations of PCBs, we found only one report of the observed concentrations of PCBs in the SoJ. The vertical profiles of dissolved CB153 concentration observed in the SoJ (Siribesi Trough) showed high value in 500 m depth, lower value in the surface layer and the depths >1000 m (Table S1) (Kannan et al., 1998). Our model results actually show a similar three layers of structure. In other seas, such as the Norwegian Sea, where deep water formation also occurs, the dissolved CB153 measurements showed a higher concentration at a depth of 200 m than in the surface layer (Lohmann et al., 2006; Sobek et al., 2004). Therefore, this model portraits a reasonable vertical structure of CB153 in the Sea of Japan.

3.2. Vertical distribution of CB153 concentration in the SoJ

To visually describe the seasonal characteristics of CB153 in the vertical direction, we present the vertical distribution of CB153 concentrations along the 131°E section (white line in Fig. 1). This section is selected as the seasonal variation of the CB153 concentration in the western Japan Basin is more pronounced and representative of that in the SoJ (Fig. 2). The three-layer vertical structure of the dissolved CB153 concentration also appears along the section (Fig. S7). As CB153 is mainly distributed in the upper 600 m, Fig. 3a–d give a close look at the dissolved CB153 concentrations from the sea surface to the 600 m layer.

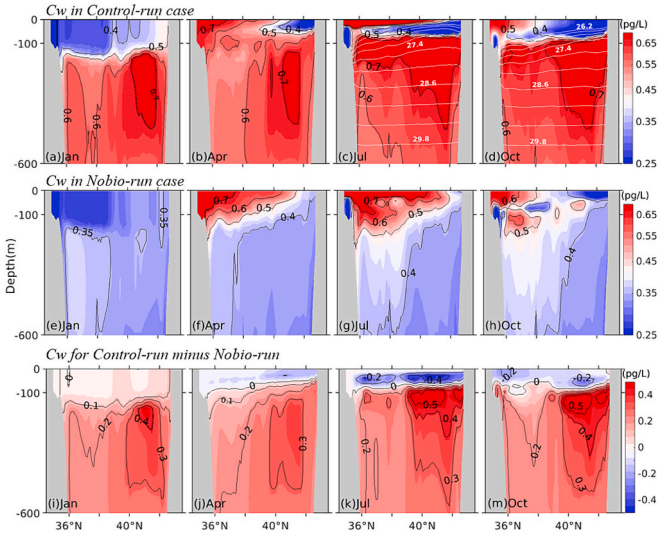

Fig. 3. Vertical distributions of dissolved CB153 concentrations (pg L^{-1}) in (a–d) control-run, (e–h) nobio-run, and (i–m) the difference of dissolved CB153 concentration between the control-run and nobio-run (control-run minus nobio-run) in the upper 600 m along 131°E section, whose position is given by the white dashed line in Fig. 1, in January, April, July, and October. The white solid lines in (c, d) denote the isopycnal lines.

In the surface layer, dissolved concentrations exhibit significant seasonality. From spring to autumn, the surface concentration is significantly higher (~0.7 pg L^{-1}) and lower (~0.4 pg L^{-1}) in the southern and northern areas of the SoJ, respectively (Fig. 3b–d). However, the dissolved concentration is higher in the northern region (~0.5 pg L^{-1}) than in the southern area in winter (~0.4 pg L^{-1}) (Fig. 3a).

In spring and summer, the atmospheric CB153 concentration is higher over the southern SoJ than over the northern SoJ (Fig. S6), which contributes to the high concentration in the southern area (Fig. 3b, c). Meanwhile, water with a high concentration of dissolved CB153 is also transported from the East China Sea to the SoJ via the Tsushima Warm Current (Fig. S1). However, this water cannot reach the northern SoJ because most of it is transported by the Tsushima Warm Current, which flows along the subpolar front at around 40°N (Fig. S1). Consequently, a low CB153 concentration is maintained in the northern region (Fig. 3b–d).

In January, although the atmospheric CB153 concentration is homogeneous over the entire SoJ, the water temperature is approximately 10 °C and 5 °C in the southern and northern SoJ (Fig. S2), respectively. Since lower water temperature favors CB153 entering the ocean from the air, we obtain a high concentration in the surface layer in the northern area (Fig. 3a).

Another feature is that there is a low-concentration in the subsurface layer from spring to autumn (Fig. 3b–d). A higher concentration of phytoplankton in the western Japan Basin in April (Fig. S3) absorbs more dissolved CB153, which results in the increase of the particulate CB153 concentration (Fig. S8) but decrease of the dissolved CB153 concentration there (Fig. 3b–d). Thereafter, the low-concentration water in the western Japan Basin is transported to the southern SoJ along the isopycnal layers (white lines in Fig. 3c, d), leading to a low concentration in the subsurface layer along the 131°E section (Fig. 3c, d).

The dissolved CB153 concentration below a depth of 100 m shows little seasonality and is twice that in the surface layer. In the area north of 40°N, there is a permanent high concentration of ~0.7 pg L^{-1} and the concentration is vertically uniform in the intermediate layer throughout the year. The concentration in the area south of 40°N is lower than that in the northern area by ~0.1 pg L^{-1}. The particulate CB153 is mainly distributed in the surface layer in the area north of 40°N in April (Fig. S8b), which is influenced by the distribution of bio-particles. Particulate CB153 does not appear in the deep layer because of the decomposition of the detritus-bound CB153.

3.3. The accumulation process of CB153 in the SoJ

The three-layer vertical structure of the dissolved CB153 concentration in the SoJ suggests that though the concentration in the surface layer is low, there is a permanently high concentration in the intermediate layer. The formation of the three-layer vertical structure and the origin of the high concentration in the intermediate layer need further examination.

Fig. 4 shows the vertical distributions of the annual mean concentration and the differences between years of dissolved CB153 along section 131°E from the first simulation year to the 21st year. The initial concentrations of the dissolved, phytoplankton, and detritus phases of PCBs in the ocean are zero in the simulation. In the 1st year, the annual mean concentration of dissolved CB153 is ~0.3 pg L^{-1} in the surface layer, and the concentration is very low at depths >100 m (Fig. 4a). With the increase in simulation time, the surface layer concentration increased slightly, suggesting that the concentration in the surface layer reached a steady state (Fig. 4b–k). The concentrations in the intermediate and deep layers continue to increase, with positive accumulation rates over the simulation time of 21 years. However, the accumulation rates change with years and depths, being high in the intermediate layer from the second to the fourth year but gradually moving to the deep layer after six years. The dissolved concentrations in the intermediate layer in the areas north and south of 40°N increase from a low value of <0.3 pg L^{-1} in the first year (Fig. 4a) to >0.7 and 0.6 pg L^{-1} in the 21st year (Fig. 4m), respectively. The concentration accumulation rate is faster in the area north of 40°N, and the highest accumulation rate appears in the Japan Basin water at this section (Fig. 4b–k). Furthermore, the dissolved concentration in the deep layer also increased from a very low value in the first year to ~0.5 pg L^{-1} in the 21st year, which reached a concentration level similar to or even higher than that in the surface layer (Fig. 4m).

To know the accumulation rate of dissolved CB153 over the entire SoJ, we calculated the mean dissolved CB153 concentration in the surface layer (0–100 m), intermediate layer (100–600 m), and deep layer (>600 m) over the 21 years (Fig. 5). The mean CB153 concentration in the surface layer shows remarkable seasonal variation with a high value in summer and a low value in winter. The seasonalities in the intermediate and deep layers are weak (Fig. 5a). The accumulation rates of dissolved CB153 in three layers decrease gradually with the simulation time (Fig. 5b). Initially, the accumulation rate is higher in the intermediate layer than in the deep layer. However, after 4 years of simulation, this rate in the deep layer exceed that of the intermediate layer. The rates in the 21st year were 0.003, 0.010, and 0.013 pg L^{-1} $year^{-1}$ in the surface, intermediate, and deep layers, respectively (Fig. 5b), which suggests that the CB153 concentration in the intermediate and deep layers will continue to increase with the extension of simulation time.

The vertical distribution of dissolved CB153 in the deep layer of SoJ is controlled by a combination of physical and biological pumps. Physical pump means that the water masses originating from continental margins transport CB153 to the deep ocean through lateral advection along the isopycnal layers and eddy diffusion. Biological pump means the transport of CB153 from the sea surface to the deep sea with the sinking of particulates, whose decomposition releases dissolved CB153 in the deep layer.

To clarify the role of physical processes on the vertical distribution of dissolved CB153 concentration in the SoJ, we examined the dissolved CB153 concentration on different density surfaces (isopycnals), which are defined by the potential density (σ1) referred to 1000 db (Fig. 6). The water above σ1 = 27.5 is in the surface layer, that of σ1 = 27.5–30.5 is in the intermediate layer, and that heavier than σ1 = 30.5 is in the deep layer. The dissolved CB153 above the σ1 = 27.5 isopycnal accumulated mainly in the area south of the subpolar front in the SoJ (Fig. 6A). On the

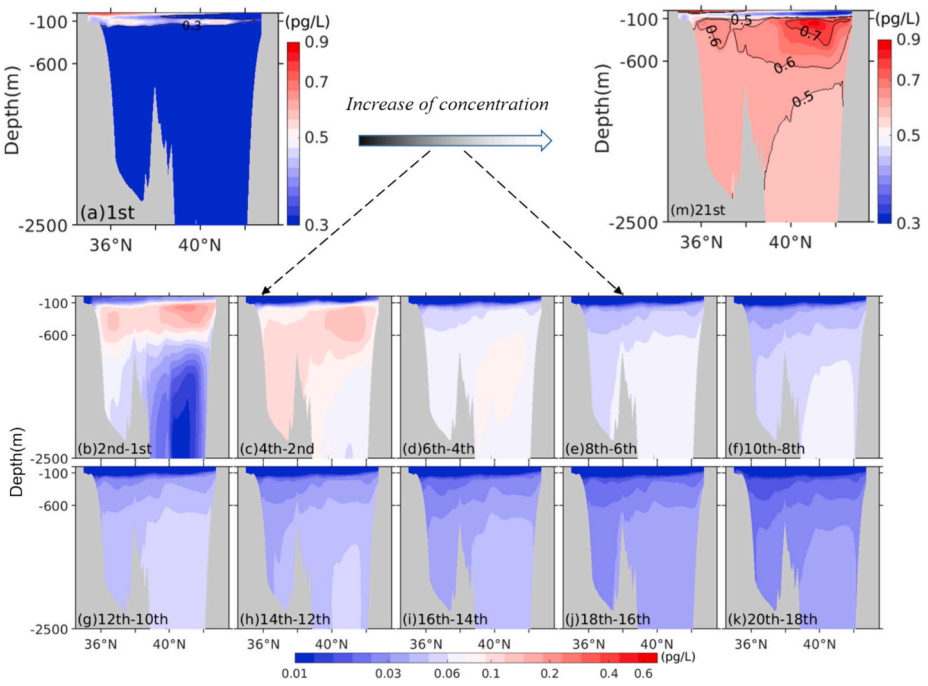

Fig. 4. Vertical distribution of the annual mean concentrations (pg L^{-1}) of dissolved CB153 in (a) the 1st year and (m) the 21st year, and (b–k) the concentration differences (pg L^{-1}) between two years such as (b) 2nd and 1st year, (c) 4th and 2nd year, (d) 6th and 4th year and so on along 131°E section. The color bar for the concentration in the 1st and 21st years is the same in (a) and (m), while that for the concentration difference between two years is also the same from (b) to (k). The black line in (b) denoted the $\sigma 1$ (potential density referred to 1000 db) along the 131°E section.

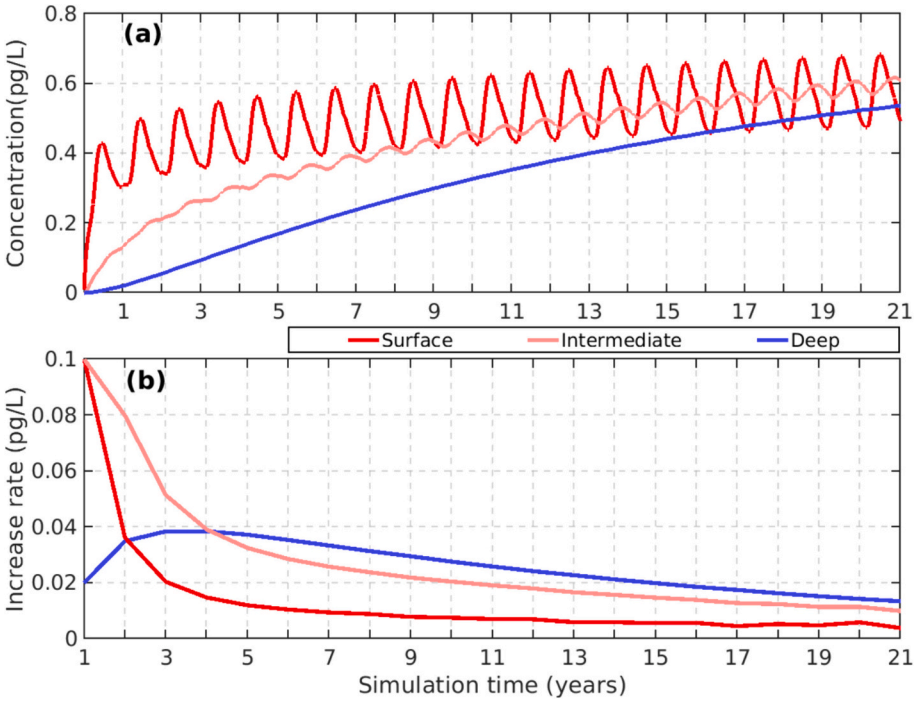

Fig. 5. Time series of (a) concentration and (b) increase rate of the dissolved CB153 concentration in the surface, intermediate, and deep layers in the SoJ during 21 years of simulation time.

σ1 = 27.7 isopycnal, the dissolved CB153 concentration increases significantly in the subpolar front region between 100 and 120 m depth (Fig. S9) owing to the sinking and remineralization of detritus-bound CB153 at this depth. The high CB153 concentration in the Japan Basin is maintained for the range of σ1 = 27.7–30.5, and the CB153 is uniformly distributed below the σ1 = 30.5 isopycnal.

In the southern SoJ, the high concentration in the surface layer originates from the Tsushima Warm Current and the strong downward air-sea exchange in summer. The streamlines of ocean currents suggest that the Tsushima Warm Current transports the CB153 to the northeastern SoJ, and this process mainly occurs above the σ1 = 27.5 isopycnal.

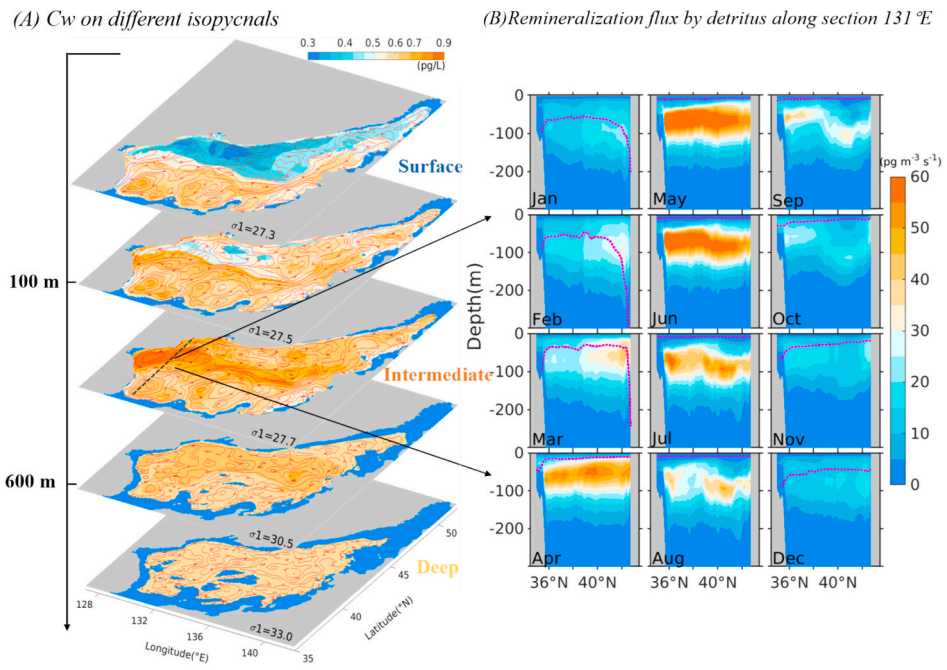

Fig. 6. (A) Distribution of dissolved CB153 concentrations at different isopycnals. The red lines with arrows denoted the streamlines of the ocean current. The black dashed line denotes 131°E section. (B) Vertical distributions of the remineralization flux from January to December along 131°E section. The magenta dashed line denotes the depth of the surface mixed layer.

Below the surface layer, there is a high CB153 concentration in the Ulleung Basin compared to the Yamato Basin, which maintains to 1000 m depth. To investigate the effect of the physical process on the accumulation of CB153 in the intermediate and deep layers, we examined the vertical current velocity (*w*) and calculated the vertical advection flux of dissolved CB153 along the zonal cross section of 37°N (the white solid line in Fig. 1). Positive and negative *w* alternately distributed along 37°N section (Fig. 7a, b). In summer, the downward *w* is prominent, especially in the western region (the Ulleung basin), where the large downward *w* is maintained from the surface layer to the layer below 1000 m. Correspondingly, the vertical advection flux of the dissolved CB153 distributes similarly to *w*, and shows significantly downward transport of dissolved CB153 in the Ulleung basin (Fig. 7c, d), which results in the higher CB153 concentration accumulation in this region as compared to the Yamato basin. The vertical advection fluxes through the depths of 100 m and 600 m were integrated in the southern SoJ and both show negative values year-round (Fig. 7e). The flux through the depth of 100 m is large in summer owing to the high CB153 concentration and large downward current velocity in summer. The flux through depth of 600 m is larger than that through depth of 100 m and shows weak seasonal variation. In addition, there are a variety of anticyclonic eddies in the southern SoJ, which also enhance the downward transport of the surface CB153 to the intermediate and deep layers. Therefore, the downward vertical advection in the southern SoJ is in favor of the accumulation of CB153 in the intermediate and deep layers in the southern SoJ.

The biological processes between dissolved and particulate CB153 in this model include the absorption by phytoplankton and detritus (Fig. S10), and the remineralization of detritus-bound CB153. The monthly remineralization flux along the 131°E section is high from March to September but lower from October to the next January, and occurs mainly in the subsurface layer (Fig. 6B). In summer and autumn, the magnitude of the flux is similar in the southern and northern SoJ, but the depth of detritus decomposition is greater in the northern region (60–140 m) than in the southern region (40–120 m). In addition to the effect of cold-water subduction in the northern area, the low water temperature in the northern region also slows down the decomposition rate of detritus. Consequently, detritus-bound CB153 can be transported to deeper layers in the northern area before decomposition.

The magenta dashed line in Fig. 3B indicates the monthly mixed layer depth (MLD), which is defined as the depth whose water temperature is 0.2 °C lower than the sea surface temperature (Miller, 1976). The MLD reaches a depth of 60 m in the majority of the SoJ from December to the next February, and is <10 m from May to September. According to the sinking velocity of detritus in the model, it can reach a depth of 6.7 m in one day. In summer, the sinking of detritus is not affected by the strong stratification and brings the detritus-bound CB153 below the mixed layer. Meanwhile, the decomposition of detritus-bound CB153 induces the accumulation of a large amount of dissolved CB153 in the subsurface layer (60–120 m). With the increase of the MLD from October to December, the previously accumulated high concentration of dissolved CB153 in the subsurface layer is mixed with the lower concentration in the surface layer. Therefore, the dissolved CB153 in the subsurface layer is diluted with the surface mixed layer. If we have a shallower MLD layer and a deeper decomposition depth of the detritus-bound CB153, the dilution rate is low. This likely occurs in the northern region, which makes the intermediate layer more prone to accumulate dissolved CB153 than in the southern region. Therefore, it is the decomposition of biogenetic particles sinking through the thermocline that transports dissolved CB153 from the surface layer to the intermediate layer, resulting in the accumulation of dissolved CB153 in the intermediate layer in the northern SoJ (Fig. 4m).

3.4. Discussion of the dominant processes controlling the accumulation of CB153

To investigate the relative contributions of physical processes and biological pump to the accumulation of CB153 in the intermediate layer of the SoJ, one sensitivity experiment was conducted. In this calculation (nobio-run), the initial and boundary conditions and the simulation time are the same as those in the control-run. However, biological processes related to CB153 are removed; therefore, only the dissolved CB153 was calculated by solving its advection and diffusion equations.

Compared to the results of the control-run (Fig. 3a–d), the vertical distribution of dissolved CB153 along the 131°E section in the nobio-run

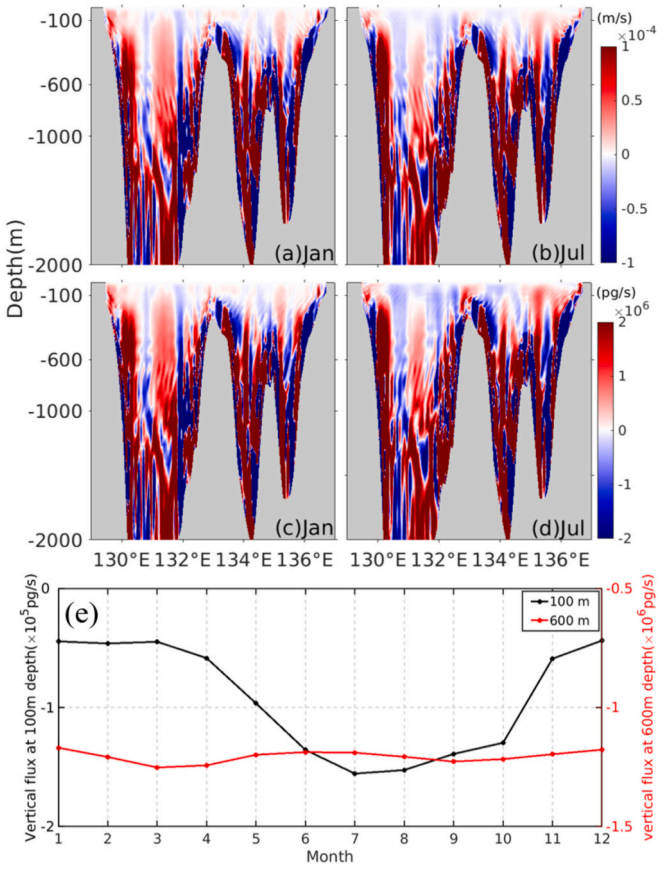

Fig. 7. Distribution of (a, b) the vertical current velocity (w), (c, d) the vertical fluxes of the dissolved CB153 along 37°N section, whose position is given by the white solid line in Fig. 1, and (e) times series of the integrated vertical fluxes of dissolved CB153 through depths of 100 m and 600 m in the southern areas of Sea of Japan. The negative (positive) w and advection flux indicate downward (upward) direction.

exhibits significant differences in the layer below 100 m depth, and these differences in the southern and northern 131°E section are inconsistent (Fig. 3e–h). In the northern area, the CB153 concentration of the intermediate layer in the nobio-run is <0.4 pg L^{-1} throughout the year. Without biological processes, the dissolved CB153 has a higher concentration in the surface layer than in the intermediate layer, suggesting that it cannot accumulate in the intermediate layer without the participation of bio-particles. Therefore, the biological process is an effective factor in controlling the accumulation of CB153 in the intermediate layer in the northern SoJ. In the southern area, however, the CB153 concentration of the intermediate layer in the nobio-run decreases less compared to the northern region. The high concentration in the southern region is maintained by the anticyclonic eddies, which results in downward transports of the surface CB153 to intermediate and deep layers in the southern SoJ.

In addition, compared to the control-run, the concentration in the surface layer is higher in the northern area than in the southern area in the nobio-run. As previously mentioned, the low concentration in the surface layer of the northern area is caused by the southwestward flowing water with a low CB153 concentration from the northernmost region. In the nobio-run, the absence of the absorption of dissolved CB153 by bio-particles results in an increase in the dissolved CB153 concentration in the surface layer of the northern region.

The concentration difference between the control-run and nobio-run is prominent in summer and autumn (Fig. 3k, m). In July, this concentration differences in the surface, intermediate, and deep layers of the northern region are ~ -0.4, ~ 0.5, and ~ 0.3 pg L^{-1}, respectively, indicating that the biological processes in the northern region remove the surface dissolved CB153 to the deeper layer, and increase the dissolved CB153 concentration in the intermediate and deep layers. The concentration difference in the surface layer of the southern region is smaller (~ -0.2 pg L^{-1}), which corresponds to the smaller increase of dissolved CB153 concentration in the deeper layer (~ 0.2 pg L^{-1}) of the southern region. Correspondingly, the contributions of biological processes to the accumulation of dissolved CB153 in the intermediate and deep layers in the northern area are approximately 70 % and 60 %, respectively, and this contribution is only 30 % in the southern area, indicating that the physical processes contribute approximately 70 % to the accumulation of dissolved CB153 in the southern SoJ. In conclusion, the biological pump plays a dominant role in the accumulation of dissolved CB153 in the intermediate layer in the northern SoJ, while the physical processes are the main factors affecting the accumulation of CB153 in the southern SoJ.

4. Conclusions

In this study, a three-dimensional hydrodynamic-ecosystem-PCB coupled model was applied to the semi-enclosed SoJ to depict the accumulation processes of dissolved CB153 in deep water and to quantitatively evaluate the relative contributions of physical processes and biological pump. To accurately characterize the accumulation processes of dissolved CB153, the model was calculated for 21 years from zero concentration for all phases of CB153. Dissolved CB153 shows significant accumulation in the Japan Basin with the highest concentration in the intermediate layer. The biological pump contributes to the accumulation of dissolved CB153 in the intermediate layer in the northern SoJ by transporting the dissolved CB153 from the surface layer through the thermocline with the sinking of biological particles that absorb the dissolved CB153 in the surface layer. The downward vertical advection in the southern SoJ contributes to the accumulation of dissolved CB153 in the intermediate and deep layers in the southern SoJ by transporting the dissolved CB153 from the surface layer to deeper layer.

Many semi-enclosed fjords exist in the global oceans (e.g., the SoJ, the Norwegian Sea, and the Labrador Sea). The PCBs concentrations are usually higher in these seas than in the open ocean. The discussion of the relative contributions of oceanic biological pump and physical processes to the accumulation of PCBs in deep water of the SoJ can be naturally tested in other semi-enclosed fjords in the future. Such studies can deepen our understanding of the regulation and diversity of accumulation mechanisms among different semi-enclosed fjords and provide fundamental information for the study of deep-sea marine fishery resources.

CRediT authorship contribution statement

Min Yang: Writing – original draft, Methodology, Conceptualization. **Xinyu Guo:** Writing – review & editing, Formal analysis, Conceptualization. **Junyong Zheng:** Writing – review & editing, Formal analysis. **Yasumasa Miyazawa:** Writing – review & editing, Formal analysis.

Declaration of competing interest

The authors declare that they have no known competing financial interests or personal relationships that could have appeared to influence the work reported in this paper.

Data availability

Most simulated data are available at https://zenodo.org/records/10360264.

Acknowledgments

The authors declare no conflicts of interest relevant to this study. We are grateful to Carey L. Friedman and Noelle Eckley Selin for providing the atmospheric PCBs data. MinYang thanks Dr. Shishun Wang for valuable suggestions on the paper. The authors also thank support from the Ministry of Education, Culture, Sports, Science and Technology, Japan (MEXT) for a project on Joint Usage/Research Center–Leading Academia in Marine and Environment Pollution Research (LaMer). This study was supported by the Grant-in-Aid for Scientific Research (MEXT KAKENHI, Grant 20KK0239), the Project of State Key Laboratory of Satellite Ocean Environment Dynamics, Second Institute of Oceanography, MNR (KJ23502G).

Appendix A. Supplementary data

Supplementary data to this article can be found online at https://doi.org/10.1016/j.scitotenv.2024.173599.

References

Abramowicz, D.A., 1990. Aerobic and anaerobic biodegradation of PCBs: a review. Crit. Rev. Biotechnol. 10, 241–251. https://doi.org/10.3109/07388559009038210.

Corsolini, S., Ademollo, N., Martellini, T., Randazzo, D., Vacchi, M., Cincinelli, A., 2017. Legacy persistent organic pollutants including PBDEs in the trophic web of the Ross Sea (Antarctica). Chemosphere 185, 699–708. https://doi.org/10.1016/j.chemosphere.2017.07.054.

Dachs, J., Lohmann, R., Ockenden, W.A., Méjanelle, L., Eisenreich, S.J., Jones, K.C., 2002. Oceanic biogeochemical controls on global dynamics of persistent organic pollutants. Environ. Sci. Technol. 36, 4229–4237. https://doi.org/10.1021/es025724k.

de Brito, A.P.X., Ueno, D., Takahashi, S., Tanabe, S., 2002. Organochlorine and butyltin residues in walleye pollock (*Theragra chalcogramma*) from Bering Sea, Gulf of Alaska and Japan Sea. Chemosphere 46, 401–411. https://doi.org/10.1016/S0045-6535(01)00183-7.

Dvoretsky, A.G., Dvoretsky, V.G., 2018. Red king crab (*Paralithodes camtschaticus*) fisheries in Russian waters: historical review and present status. Rev. Fish Biol. Fish. 28, 331–353. https://doi.org/10.1007/s11160-017-9510-1.

Friedman, C.L., Selin, N.E., 2016. PCBs in the Arctic atmosphere: determining important driving forces using a global atmospheric transport model. Atmos. Chem. Phys. 16, 3433–3448. https://doi.org/10.5194/acp-16-3433-2016.

Froescheis, O., Looser, R., Cailliet, G.M., Jarman, W.M., Ballschmiter, K., 2000. The deep-sea as a final global sink of semivolatile persistent organic pollutants? Part I: PCBs in surface and deep-sea dwelling fish of the North and South Atlantic and the Monterey Bay Canyon (California). Chemosphere 40, 651–660. https://doi.org/10.1016/S0045-6535(99)00461-0.

Gamo, T., Nakayama, N., Takahata, N., Sano, Y., Zhang, J., Yamazaki, E., Taniyasu, S., Yamashita, N., 2014. The sea of Japan and its unique chemistry revealed by time-series observations over the last 30 years. Monogr. Environ. Earth Planets 2, 1–22. https://doi.org/10.5047/meep.2014.00201.0001.

Isobe, A., 2020. Paleo-ocean destratification triggered by the subduction of the Oyashio water into the sea of Japan after the last glacial maximum. Paleoceanogr. Paleoclimatology 35, e2019PA003593. https://doi.org/10.1029/2019PA003593.

Jamieson, A.J., Malkocs, T., Piertney, S.B., Fujii, T., Zhang, Z., 2017. Bioaccumulation of persistent organic pollutants in the deepest ocean fauna. Nat. Ecol. Evol. 1, 1–4. https://doi.org/10.1038/s41559-016-0051.

Jepson, P.D., Deaville, R., Barber, J.L., Aguilar, À., Borrell, A., Murphy, S., Barry, J., Brownlow, A., Barnett, J., Berrow, S., Cunningham, A.A., Davison, N.J., ten Doeschate, M., Esteban, R., Ferreira, M., Foote, A.D., Genov, T., Giménez, J., Loveridge, J., Llavona, Á., Martin, V., Maxwell, D.L., Papachlimitzou, A., Penrose, R., Perkins, M.W., Smith, B., de Stephanis, R., Tregenza, N., Verborgh, P., Fernandez, A., Law, R.J., 2016. PCB pollution continues to impact populations of orcas and other dolphins in European waters. Sci. Rep. 6, 18573 https://doi.org/10.1038/srep18573.

Jurado, E., Jaward, F.M., Lohmann, R., Jones, K.C., Simó, R., Dachs, J., 2004. Atmospheric dry deposition of persistent organic pollutants to the Atlantic and inferences for the global oceans. Environ. Sci. Technol. 38, 5505–5513. https://doi.org/10.1021/es049240v.

Jurado, E., Jaward, F., Lohmann, R., Jones, K.C., Simó, R., Dachs, J., 2005. Wet deposition of persistent organic pollutants to the global oceans. Environ. Sci. Technol. 39, 2426–2435. https://doi.org/10.1021/es048599g.

Kanawa, K., Yamoto, H., Mitamura, H., Arai, N., Ohtani, T., Ozaki, T., 2014. <Poster session>snow crab behaviors in the deep-sea floor revealed by VPS. In: 20th Symposium of the International Society on Biotelemetry Proceedings, pp. 97–99.

Kannan, N., Yamashita, N., Petrick, G., Duinker, J.C., 1998. Polychlorinated biphenyls and nonylphenols in the sea of Japan. Environ. Sci. Technol. 32, 1747–1753. https://doi.org/10.1021/es970713q.

Lee, T., Hyun, J.-H., Mok, J.S., Kim, D., 2008. Organic carbon accumulation and sulfate reduction rates in slope and basin sediments of the Ulleung Basin, East/Japan Sea. Geo-Mar. Lett. 28, 153–159. https://doi.org/10.1007/s00367-007-0097-8.

Lohmann, R., Jurado, E., Pilson, M.E.Q., Dachs, J., 2006. Oceanic deep water formation as a sink of persistent organic pollutants. Geophys. Res. Lett. 33 https://doi.org/10.1029/2006GL025953.

Maldonado, C., Bayona, J.M., 2002. Organochlorine compounds in the North-Western Black Sea water: distribution and water column process. Estuar. Coast. Shelf Sci. 54, 527–540. https://doi.org/10.1006/ecss.2000.0672.

Miller, J.R., 1976. The salinity effect in a mixed layer ocean model. J. Phys. Oceanogr. 6, 29–35. https://doi.org/10.1175/1520-0485(1976)006<0029:TSEIAM>2.0.CO;2.

Miyazawa, Y., Varlamov, S.M., Miyama, T., Guo, X., Hihara, T., Kiyomatsu, K., et al., 2017. Assimilation of high-resolution sea surface temperature data into an operational nowcast/forecast system around Japan using a multi-scale three-dimensional variational scheme. Ocean Dyn. 67 (6), 713–728. https://doi.org/10.1007/s10236-017-1056-1.

Oba, T., Irino, T., 2012. Sea level at the last glacial maximum, constrained by oxygen isotopic curves of planktonic foraminifera in the Japan Sea. J. Quat. Sci. 27, 941–947. https://doi.org/10.1002/jqs.2585.

Schulz-Bull, D.E., Petrick, G., Bruhn, R., Duinker, J.C., 1998. Chlorobiphenyls (PCB) and PAHs in water masses of the northern North Atlantic. Mar. Chem. 61, 101–114. https://doi.org/10.1016/S0304-4203(98)00010-3.

Sinkkonen, S., Paasivirta, J., 2000. Degradation half-life times of PCDDs, PCDFs and PCBs for environmental fate modeling. Chemosphere 40, 943–949. https://doi.org/10.1016/S0045-6535(99)00337-9.

Sobek, A., Gustafsson, Ö., 2014. Deep water masses and sediments are main compartments for polychlorinated biphenyls in the Arctic Ocean. Environ. Sci. Technol. 48, 6719–6725. https://doi.org/10.1021/es500736q.

Sobek, A., Gustafsson, Ö., Hajdu, S., Larsson, U., 2004. Particle–water partitioning of PCBs in the photic zone: a 25-month study in the open Baltic Sea. Environ. Sci. Technol. 38, 1375–1382. https://doi.org/10.1021/es034447u.

Storelli, M.M., Losada, S., Marcotrigiano, G.O., Roosens, L., Barone, G., Neels, H., Covaci, A., 2009. Polychlorinated biphenyl and organochlorine pesticide contamination signatures in deep-sea fish from the Mediterranean Sea. Environ. Res. 109, 851–856. https://doi.org/10.1016/j.envres.2009.07.008.

Sun, C., Soltwedel, T., Bauerfeind, E., Adelman, D.A., Lohmann, R., 2016. Depth profiles of persistent organic pollutants in the north and tropical Atlantic Ocean. Environ. Sci. Technol. 50, 6172–6179. https://doi.org/10.1021/acs.est.5b05891.

Takahashi, S., Karri, R., Tanabe, S., 2014. Contamination by persistent organic pollutants and related compounds in deep-sea ecosystems along frontal zones around Japan. In: The Handbook of Environmental Chemistry. Springer, Berlin Heidelberg, Berlin, Heidelberg. https://doi.org/10.1007/698_2013_252.

Ueno, D., Takahashi, S., Tanaka, H., Subramanian, A.N., Fillmann, G., Nakata, H., Lam, P.K.S., Zheng, J., Muchtar, M., Prudente, M., Chung, K.H., Tanabe, S., 2003. Global pollution monitoring of PCBs and organochlorine pesticides using skipjack tuna as a bioindicator. Arch. Environ. Contam. Toxicol. 45, 378–389. https://doi.org/10.1007/s00244-002-0131-9.

Wagner, C.C., Amos, H.M., Thackray, C.P., Zhang, Y., Lundgren, E.W., Forget, G., Friedman, C.L., Selin, N.E., Lohmann, R., Sunderland, E.M., 2019. A global 3-D ocean model for PCBs: benchmark compounds for understanding the impacts of global change on neutral persistent organic pollutants. Glob. Biogeochem. Cycles 33, 469–481. https://doi.org/10.1029/2018GB006018.

Yanagi, T., 2002. Water, salt, phosphorus and nitrogen budgets of the Japan Sea. J. Oceanogr. 58, 797–804. https://doi.org/10.1023/A:1022815027968.

Yang, M., Guo, X., Ishizu, M., Miyazawa, Y., 2022. The Kuroshio regulates the air–sea exchange of PCBs in the Northwestern Pacific Ocean. Environ. Sci. Technol. 56, 12307–12314. https://doi.org/10.1021/acs.est.2c03459.

Yosho, I., Hirose, T., Shirai, S., 2009. Bathymetric distribution of beni-zuwai crab *Chionoecetes japonicus* in the northern part of the sea of Japan. Fish. Sci. 75, 1417–1429. https://doi.org/10.1007/s12562-009-0169-y.

Zhang, L., Thibodeaux, L., Jones, L., Lohmann, R., 2015. Simulation of observed PCBs and pesticides in the water column during the North Atlantic bloom experiment. Environ. Sci. Technol. 49, 13760–13767. https://doi.org/10.1021/acs.est.5b00223.

Zhang, J., Ma, Y., Zhong, Y., Lohmann, R., 2023. Combined effects of fronts, upwelling and the biological pump on organophosphate esters in the Changjiang (Yangtze) river estuary during summer. J. Geophys. Res. Oceans 128, e2023JC020081. https://doi.org/10.1029/2023JC020081.